

Superexchange theory of electronic polarization driven by relativistic spin-orbit interaction at the half-filling

I. V. Solovyev^{1,2,*}

¹*International Center for Materials Nanoarchitectonics,
National Institute for Materials Science,
1-1 Namiki, Tsukuba, Ibaraki 305-0044, Japan*

²*Department of Theoretical Physics and Applied Mathematics,
Ural Federal University, Mira str. 19, 620002 Ekaterinburg, Russia*

(Dated: September 16, 2018)

Abstract

By applying Berry-phase theory for the effective half-filled Hubbard model, we derive an analytical expression for the electronic polarization driven by the relativistic spin-orbit (SO) coupling. The model itself is constructed in the Wannier basis, using the input from the first-principles electronic structure calculations in the local-density approximation, and then treated in the spirit of the superexchange theory. The obtained polarization has the following form: $\mathbf{P}_{ij} = \epsilon_{ji} \mathcal{P}_{ij} \cdot [\mathbf{e}_i \times \mathbf{e}_j]$, where ϵ_{ji} is the direction of the bond $\langle ij \rangle$, \mathbf{e}_i and \mathbf{e}_j are the directions of spins in this bond, and \mathcal{P}_{ij} is the pseudovector containing all the information about the crystallographic symmetry of the considered system. The expression describes the ferroelectric activity in various magnets with non-collinear but otherwise nonpolar magnetic structures, which would yield no polarization without SO interaction, including the magnetoelectric (ME) effect, caused by the ferromagnetic canting of spins in the external magnetic field, and spin-spiral multiferroics. The abilities of this theory are demonstrated for the analysis of linear ME effect in Cr_2O_3 and BiFeO_3 and properties multiferroic MnWO_4 and $\beta\text{-MnO}_2$. In all considered examples, the theory perfectly describes the symmetry properties of the induced polarization. However, in some cases, the values of this polarization are underestimated, suggesting that other effects, besides the spin and electronic ones, can also play an important role.

* SOLOVYEV.Igor@nims.go.jp

I. INTRODUCTION

The relativistic spin-orbit (SO) interactions is responsible for many spectacular phenomena in condensed matter physics, which are widely employed in many technological applications. Particularly, being a natural mechanism connecting spin and orbital degrees of freedom, it provides a unique possibility for the mutual control of various spin and lattice-related properties. Every year, growing interest in this problem leads to the discovery new and more sophisticated schemes of such control [1].

One of the interesting topics is the effects of the SO coupling in noncentrosymmetric substances. In magnetic systems, it leads to the famous antisymmetric Dzyaloshinskii-Moriya (DM) interaction $\mathbf{d}_{ij} \cdot [\mathbf{e}_i \times \mathbf{e}_j]$ between spins in the noncentrosymmetric bond $\langle ij \rangle$, where \mathbf{e}_i and \mathbf{e}_j are the directions of these spins [2, 3]. The DM interaction is generally responsible for the noncollinear spin order. Alternatively, in some magnetic architectures, the noncollinear alignment of spins can break the inversion symmetry, which will be immediately manifested in the ferroelectric (FE) activity. The classical example of such activity is the magnetoelectric (ME) effect, where the noncollinearity is induced by the external magnetic field [4]. The interest in this problem has reemerged a decade ago, after the discovery of new generation of multiferroic materials, where the inversion symmetry is broken by some complex and, in many cases, noncollinear magnetic order [5]. Nevertheless, the microscopic understanding of mechanisms resulting in finite electric polarization in this case is still far from being complete, even despite of significant progress in this direction.

Historically, the first phenomenological expression for the electric polarization, which can be induced by a noncollinear spin order, was introduced by Moriya in 1968 on the basis of general symmetry considerations [6]. In each magnetic bond, such polarization has the form:

$$P_{ij}^a = \sum_b \mathfrak{d}_{ij}^{ab} [\mathbf{e}_i \times \mathbf{e}_j]^b, \quad (1)$$

which is similar to the expression for DM exchange interaction, where the vector \mathbf{d}_{ij} is replaced by the tensor \mathfrak{d}_{ij}^{ab} with a and b denoting x , y , or z .

The microscopic derivation of expression for the electric polarization, which is driven by the relativistic SO coupling in noncollinear magnetic substances, was given in Ref. [7]. However, it should be understood that the microscopic model considered Ref. [7] deals with very special example of electronic structure of the transition-metal (TM) oxides, consisting

of the t_{2g} levels with some particular scheme of filling, which are split by the SO coupling and interact via intermediate oxygen (O) states in the single undistorted TM-O-TM bond. Thus, the analysis is hardly to be complete. Nevertheless, on the basis of these considerations, the authors of Ref. [7] have concluded that the electric polarization should behaves as

$$\mathbf{P}_{ij} \propto \boldsymbol{\epsilon}_{ji} \times [\mathbf{e}_i \times \mathbf{e}_j], \quad (2)$$

where $\boldsymbol{\epsilon}_{ji}$ is the unit vector in the direction of TM site j relative to the TM site i . It is referred to as the spin-current mechanism of the electric polarization, which is widely used today for the analysis of experimental data [5]. Similar conclusion was drawn in Ref. [8], being based on the phenomenological Ginzburg-Landau theory. The expression (2) does not depend on the specific crystallographic symmetry of the considered system, so that one can have a wrong impression that the electric polarization in all noncollinear magnets should behave in a similar way. Nevertheless, this expression is formally consistent with the general definition (1), given by Moriya, and can be reduced to it by introducing the tensor $\mathfrak{d}_{ij}^{ab} = -\varepsilon_{abc}\epsilon_{ji}^c$, where ε_{abc} is the antisymmetric symbol of Levi-Civita. It is often claimed that the microscopic mechanism responsible for such behavior is similar to the inverse DM mechanism, proposed in Ref. [9]: similar to what how the off-centrosymmetric oxygen displacement in the bond TM-O-TM gives rise to the noncollinear alignment of spins [2, 3], one can expect the opposite (magnetostrictive-like) effect, where the noncollinear magnetic alignment should lead to the off-centrosymmetric atomic displacement responsible for the additional magnetic energy gain: $\sum_{ij} \mathbf{d}_{ij} \cdot [\mathbf{e}_i \times \mathbf{e}_j]$. However, it should be understood that these mechanisms are quite different (though complementary to each other): Ref. [7] deals with the purely electronic effect, while Ref. [9] deals with the lattice effect.

The most rigorous theoretical basis for the analysis of electronic polarization is provided by the Berry-phase theory, which relates the polarization with the expectation value of the position operator in the state specified by localized Wannier functions [10–12]:

$$\mathbf{P} = -\frac{e}{V} \int \mathbf{r} w^2(\mathbf{r}) d\mathbf{r}, \quad (3)$$

where $-e < 0$ is the electron charge, V is the unit-cell volume, and $w^2(\mathbf{r}) = \sum_{n=1}^M |W_n(\mathbf{r})|^2$ is the total weight of Wannier functions for the M occupied states. Each Wannier function is centered near certain site of the lattice and can have tails spreading to the neighboring sites. The relative weight of these tails depends on the magnetic state. This is how the

Wannier function bears the information about the magnetic configuration at the neighboring sites. Thus, the understanding of magnetic-state dependence of the electronic polarization is essentially the understanding of how the magnetic order and relativistic SO interaction leads to the asymmetric deformation of the Wannier functions around each magnetic site [13–15]. It should not be confused with the asymmetric distribution of the electron density at each magnetic site, because the electron density is a superposition of the weights of the Wannier functions centered at this and neighboring sites, which can lead to the incorrect answer [10, 11].

In our previous work [14] we have applied this strategy to the analysis of electronic polarization caused by the nonrelativistic double exchange mechanism. In that case, competing magnetic interactions of both relativistic and nonrelativistic origin result in highly asymmetric magnetic structure, which breaks the inversion symmetry. The SO interaction plays an important role in this asymmetry: for instance, it is responsible for the single-ion anisotropy, which deforms the homogeneous spin-spiral texture in multiferroic manganites [14, 16] (the so-called bunching effect [17]). This deformation gives rise to the polarization $\mathbf{P}_{ij} \propto (\mathbf{e}_i \cdot \mathbf{e}_j)$, which depends on the SO coupling only indirectly, via the noncentrosymmetric distribution of the directions of spins, while the proportionality coefficient between \mathbf{P}_{ij} and $(\mathbf{e}_i \cdot \mathbf{e}_j)$ does not depend on the SO coupling. This double exchange mechanism has allowed us to rationalize many aspects of the behavior of electric polarization in multiferroic manganites [14].

In this article we consider the proper spin-current mechanism. In some sense, the situation is the opposite to the double exchange mechanism, considered in Ref. [14]. Namely, we will deal with some noncollinear magnetic structures, which are stabilized by nonrelativistic means: it can be either the spin-spiral structure arising from the competition of several isotropic exchange interactions or a canted spin structure, inherent to the ME effect, where the the collinear antiferromagnetic (AFM) order is deformed by the external magnetic field. Without SO coupling all these magnetic structures can be transformed to themselves by combining the spacial inversion with some appropriate rotation of the spin system as the whole [18]. Therefore, the electric polarization will vanish. Nevertheless, the situation may change after switching on the SO coupling, which does not deform the spin texture itself (or, at least, such deformation can be neglected), but can deform the Wannier functions, resulting in their asymmetry and finite electronic polarization.

Our analysis will be applied to the effective Hubbard model derived from the first-

principles electronic structure calculations and using the local-density approximation (LDA) as the starting point for such derivation [19]. We consider the simplest case of the half-filling, which also allows us to get rid of additional complications related to the orbital degrees of freedom. Furthermore, the on-site Coulomb repulsion is the largest parameter in our model, so that other parameters can be treated as a perturbation in the spirit of the superexchange (SE) theory [20]. We will use this strategy in order to derive an analytical expression for the DM exchange interactions and electronic polarization. We will show that the correct expression for electronic polarization, which driven by the spin-current mechanism in the framework of the Berry-phase theory [10, 11], has the following form:

$$\mathbf{P}_{ij} = \epsilon_{ji} \mathcal{P}_{ij} \cdot [\mathbf{e}_i \times \mathbf{e}_j], \quad (4)$$

where the pseudovector \mathcal{P}_{ij} contains all the information about the individual symmetry of the lattice. Thus, there is at least one important addition to the phenomenological expression (2): the polarization does depend on the symmetry of the lattice, as it should be. Moreover, the functional dependence is different and there is no direct coupling between ϵ_{ji} and $[\mathbf{e}_i \times \mathbf{e}_j]$. Furthermore, by defining $\mathfrak{d}_{ij}^{ab} = \epsilon_{ji}^a \mathcal{P}_{ij}^b$, it is also straightforward to see the form of this expression is consistent with Eq. (1), proposed by Moriya [6]. We will show that this expression is very general and describes not only the behavior of polarization in the spin-spiral magnets, but also the ME effect, caused by the ferromagnetic (FM) canting of spins in otherwise collinear AFM states of a special symmetry, which is not captured by phenomenological Eq. (2).

Another important issue is whether the spin-current mechanism alone is able to reproduce experimental values of the ME effect and electric polarization in real materials. Additional mechanisms, which are widely discussed in the literature, are the lattice deformation [21–23] (in line with the proposal [9]), orbital contribution to the ME coupling [22, 24], and hidden deformation of the magnetic texture with broken inversion symmetry [16, 18]. By using realistic model, derived from the first-principles calculations, we will show that the situation can be very different: In some cases, the spin-current mechanism alone reproduces the experimental polarization reasonably well. In other cases (e.g., in Cr_2O_3), it captures only the symmetry properties of the polarization, while the numerical values can be off by several order of magnitude, suggesting the importance of other mechanisms [22–24].

The rest of the article is organized as follows. In Sec. II we will present our formalism

based on the SE theory, which is applied to antisymmetric DM exchange interactions and electric polarization in Secs. II A and II B, respectively. The details of these derivations are given in the Supplemental Material [25]. In Sec. III we will consider practical applications of this formalism to the linear ME effect in Cr_2O_3 and BiFeO_3 (Secs. III A and III B, respectively) and FE activity caused by the spin-spiral order in multiferroic MnWO_4 and $\beta\text{-MnO}_2$ (Sec. III C and III D, respectively). Finally, in Sec. IV, we will summarize our work.

II. FORMALISM

In this section we will sketch the main details of derivation of analytical expressions for the DM exchange interactions and electric polarization, following the SE theory in the lowest order of perturbation with respect to the transfer integrals \hat{t}_{ij} [20]. The technical details can be found in the Supplemental Material [25]. The simplest microscopic model, capturing the physics of the spin-current mechanism, reads $\hat{H} = \hat{h} + \hat{t}$, where $\hat{h} \equiv \hat{h}_{\text{ex}} + \hat{h}_{\text{cf}} + \hat{h}_{\text{so}}$ is the on-site part, including the interaction $\hat{h}_{\text{ex}} = \frac{U}{2}\mathbf{e} \cdot \hat{\boldsymbol{\sigma}}$ with the internal exchange field in the direction $\mathbf{e} = (\sin\theta\cos\phi, \sin\theta\sin\phi, \cos\theta)$ ($\hat{\boldsymbol{\sigma}}$ being the vector of Pauli matrices), the crystal-field splitting \hat{h}_{cf} , and the SO interaction $\hat{h}_{\text{so}} = \frac{\xi}{2}\hat{\mathbf{L}} \cdot \hat{\boldsymbol{\sigma}}$, while $\hat{t} \equiv [\hat{t}_{ij}]$ is the inter-site part. More specifically, \hat{H} can be viewed as a mean-field Hamiltonian (for instance, the one obtained from the solution of the Hubbard model in the Hartree-Fock approximation), where \hat{h}_{ex} describes the averaged exchange splitting for the half-filled ionic shell, driven by the effective interaction U , and the crystal field \hat{h}_{cf} also includes the effects of nonsphericity of the Coulomb and exchange potential. The form of \hat{h}_{ex} implies that spins are decoupled from the orbital degrees of freedom, which do not adjust the reorientation of spins. Thus, what we consider here is the canonical “spin-current” model, which include direct contributions of the orbital magnetization in neither DM interactions nor electric polarization. Parameters of such microscopic model, formulated in the Wannier basis [12], can be derived from the first-principles electronic structure calculations [19]. For practical purposes we use the linear muffin-tin orbital (LMTO) method [26].

The basic idea of the SE theory is to start from the atomic limit and treat \hat{h}_{so} and \hat{t} as a perturbation. Then, the wavefunctions of $\hat{H}_0 = \hat{h}_{\text{ex}} + \hat{h}_{\text{cf}}$ for the occupied the occupied (–)

and unoccupied (+) spin states are given by

$$|\Psi^-\rangle = \begin{pmatrix} -\sin \frac{\theta}{2} e^{-i\phi} \\ \cos \frac{\theta}{2} \end{pmatrix} |\Psi\rangle$$

and

$$|\Psi^+\rangle = \begin{pmatrix} \cos \frac{\theta}{2} \\ \sin \frac{\theta}{2} e^{i\phi} \end{pmatrix} |\Psi\rangle,$$

respectively, where $|\Psi\rangle$ is the column of eigenvectors of \hat{h}_{cf} with the eigenvalues $\{\varepsilon_n\}$. More specifically, $|\Psi\rangle$ is the M -dimensional vector in the subspace of orbital states, while $|\Psi^\pm\rangle$ are $2M$ -dimensional vectors in the space of spin and orbital states. Then, corresponding eigenvectors in the first order of the SO interaction will be given by

$$|\tilde{\Psi}^-\rangle = |\Psi^-\rangle - \bar{\xi} |\Psi^+\rangle \langle \Psi^+ | \left(\hat{\mathbf{L}} - [\hat{h}_{\text{cf}}, \hat{\mathbf{L}}] \right) \cdot \hat{\mathbf{S}} |\Psi^-\rangle$$

and

$$|\tilde{\Psi}^+\rangle = |\Psi^+\rangle + \bar{\xi} |\Psi^-\rangle \langle \Psi^- | \left(\hat{\mathbf{L}} + [\hat{h}_{\text{cf}}, \hat{\mathbf{L}}] \right) \cdot \hat{\mathbf{S}} |\Psi^+\rangle,$$

where $\bar{\xi} = \xi/U$, $\hat{h}_{\text{cf}} = \hat{h}_{\text{cf}}/U$, and $[\hat{A}, \hat{B}] = \hat{A}\hat{B} - \hat{B}\hat{A}$. Moreover, in the conventional perturbation theory expression, we further expand $(\varepsilon_n - \varepsilon_m \pm U)^{-1}$ with respect to \hat{h}_{cf} . Then, the first terms in (...) correspond to $\hat{h}_{\text{cf}} = \text{const}$ (the constant energy shift), while the second terms appear in the first order of \hat{h}_{cf} . In practical calculations, we use the effective ξ , which also incorporates the change of the Coulomb and exchange potential in the first order of the SO interaction, as obtained in the self-consistent linear response (SCLR) theory [27].

A. Exchange Interactions

The exchange interactions in the bond $\langle ij \rangle$ describe the energy change δE_{ij} in the second order of $\hat{t}_{ij} = \hat{t}_{ij}/U$, where the transfer integrals connect the occupied and unoccupied states of the sites i and j :

$$\delta E_{ij} \simeq -U \langle \tilde{\Psi}_i^- | \hat{t}_{ij} + \frac{1}{2} [\hat{h}_{\text{cf}}, \hat{t}_{ij}] | \tilde{\Psi}_j^+ \rangle \langle \tilde{\Psi}_j^+ | \hat{t}_{ji} - \frac{1}{2} [\hat{h}_{\text{cf}}, \hat{t}_{ji}] | \tilde{\Psi}_i^- \rangle + (i \leftrightarrow j).$$

This expression is also valid in the first order of \hat{h}_{cf} . Then, after tedious but rather straightforward algebra, it can be rearranged as (see Ref. [25] for details)

$$\delta E_{ij} \simeq J_{ij} (1 - \mathbf{e}_i \cdot \mathbf{e}_j) + \mathbf{d}_{ij} \cdot [\mathbf{e}_i \times \mathbf{e}_j], \quad (5)$$

where

$$J_{ij} = -U \text{Tr}_L \left\{ \hat{t}_{ij} \hat{t}_{ji} \right\} \quad (6)$$

is the isotropic exchange coupling, which does not depend on the SO interaction, and

$$\mathbf{d}_{ij} = \xi \text{Tr}_L \left\{ \hat{t}_{ij} [[\hat{h}_{\text{cf}}, i\hat{\mathbf{L}}], \hat{t}_{ji}] \right\} \quad (7)$$

is the DM coupling, which appears in the first order of the SO interaction. Other exchange interactions, including the symmetric anisotropic one, appear only in higher orders of the SO coupling. Tr_L in Eqs. (6) and (7) denotes the trace over M orbital indices.

Finally, we note the following properties:

- (i) \mathbf{d}_{ij} is the antisymmetric pseudovector: $\hat{I}\mathbf{d}_{ij} = \mathbf{d}_{ij}$, and $\mathbf{d}_{ji} = -\mathbf{d}_{ij}$;
- (ii) The values of the DM interactions depend on the crystal-field splitting and vanish when $\hat{h}_{\text{cf}} = \text{const.}$ Then, Eq. (7) can be interpreted in the following way: since $[\hat{h}_{\text{cf}}, i\hat{\mathbf{L}}]$ is the measure of unquenched orbital magnetization (or the observable orbital magnetization in the presence of the crystal field), the DM interactions \mathbf{d}_{ij} is a probe of the orbital magnetization at the site j by the electron hoppings from the site i (and vice versa).

B. Electronic Polarization

We start with the general expression for the electric polarization (3) in terms of the Wannier functions for the occupied states. Moreover, we adopt it for the lattice model and assume that all weights of w are localized in the lattice points: i.e., if w_i are occupied Wannier functions centered at the site i , their weights are distributed as

$$w_i^2(\mathbf{r}) = \sum_j w_{ij}^2 \delta(\mathbf{r} - \Delta\boldsymbol{\tau}_{ji}),$$

where $\Delta\boldsymbol{\tau}_{ji} = \mathbf{R}_j - \mathbf{R}_i$ is the position of the site j relative to the site i . Then, the electronic polarization (3) can be related to the asymmetric transfer of the weights of the Wannier functions in each bond [14]:

$$\mathbf{P} = \frac{1}{2} \sum_{ij} \mathbf{P}_{ij}, \quad (8)$$

where

$$\mathbf{P}_{ij} = -\frac{e\Delta\boldsymbol{\tau}_{ji}}{V} (w_{ij} - w_{ji}). \quad (9)$$

In the SE theory, the quantities w_{ij} are evaluated in the first order of perturbation theory for the Wannier functions with respect to \hat{t}_{ij} , starting from the atomic limit:

$$w_{ij} \simeq |\langle \tilde{\Psi}_j^+ | \hat{t}_{ji} - [\hat{h}_{\text{cf}}, \hat{t}_{ji}] | \tilde{\Psi}_i^- \rangle|^2.$$

Then, using tedious but rather straightforward algebra, one can obtain the following expression for \mathbf{P}_{ij} (see Ref. [25] for details):

$$\mathbf{P}_{ij} = \frac{e\Delta\tau_{ji}}{V} \bar{\xi} \text{Tr}_L \left\{ [\hat{h}_{\text{cf}}, \hat{t}_{ij}] [[\hat{h}_{\text{cf}}, i\hat{\mathbf{L}}], \hat{t}_{ji}] + [\hat{h}_{\text{cf}}, \hat{t}_{ji}] [[\hat{h}_{\text{cf}}, i\hat{\mathbf{L}}], \hat{t}_{ij}] \right\} \cdot [\mathbf{e}_i \times \mathbf{e}_j], \quad (10)$$

which can be further rearranged as Eq. (4) with $\boldsymbol{\epsilon}_{ji} = \frac{\Delta\tau_{ji}}{|\Delta\tau_{ji}|}$ and

$$\mathcal{P}_{ij} = \frac{e|\Delta\tau_{ji}|}{V} \bar{\xi} \text{Tr}_L \left\{ [\hat{h}_{\text{cf}}, \hat{t}_{ij}] [[\hat{h}_{\text{cf}}, i\hat{\mathbf{L}}], \hat{t}_{ji}] + [\hat{h}_{\text{cf}}, \hat{t}_{ji}] [[\hat{h}_{\text{cf}}, i\hat{\mathbf{L}}], \hat{t}_{ij}] \right\}.$$

Thus, we note the following:

- (i) Unlike \mathbf{d}_{ij} , \mathcal{P}_{ij} is the *symmetric* pseudovector: $\hat{I}\mathcal{P}_{ij} = \mathcal{P}_{ij}$, while $\mathcal{P}_{ji} = \mathcal{P}_{ij}$, where the latter property comes from the definition of \mathbf{P}_{ij} [Eq. (9)];
- (ii) Similar to the DM interactions, the electronic polarization crucially depends on \hat{h}_{cf} and vanishes when $\hat{h}_{\text{cf}} = \text{const}$;
- (iii) There is a fundamental difference from phenomenological expression (2) [7, 8]. Namely, the spin-dependent cross product $[\mathbf{e}_i \times \mathbf{e}_j]$ does not couple directly to $\boldsymbol{\epsilon}_{ji}$. It couples to the pseudovector \mathcal{P}_{ji} , which contains all the information about particular crystallographic symmetry of the considered system. The directional dependence of \mathbf{P} is specified by the vectors $\boldsymbol{\epsilon}_{ji}$, which are modulated by the scalar products $\mathcal{P}_{ij} \cdot [\mathbf{e}_i \times \mathbf{e}_j]$. This important addition will allow us to resolve several controversies related to the symmetry properties of the electric polarization induced by the noncollinear magnetic alignment.

III. RESULTS AND DISCUSSIONS

A. Perpendicular Magnetoelectric Effect in Cr_2O_3

We start our discussion with the canonical example of ME effect in antiferromagnetic Cr_2O_3 [4], which crystallizes in the corundum structure (the space group is $R\bar{3}c$) [28]. The formal configuration of the Cr-ions in Cr_2O_3 is $3d^3$. According to the electronic structure calculations in LDA, Cr_2O_3 has well isolated Cr t_{2g} band near the Fermi level, which accommodates 3 electrons per one Cr site (Fig. 1). Thus, as a first approximation, we consider

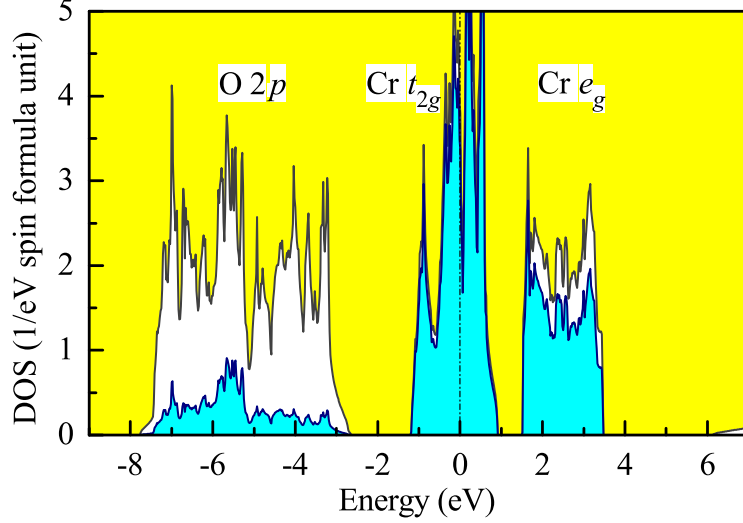


FIG. 1. (Color online) Total and partial densities of states of Cr_2O_3 in the local density approximation. The shaded light (blue) area shows contributions of the Cr 3d states. Positions of the main bands are indicated by symbols. The Fermi level is at zero energy (shown by dot-dashed line).

the simplest t_{2g} model at the half filling and try to apply this model for the analysis of the ME effect in Cr_2O_3 . The model itself has been constructed in the basis of Wannier functions, and the parameters of this model have been derived as described in Ref. [19]. The obtained transfer integrals and the crystal-field splitting perfectly reproduce Cr t_{2g} band structure in LDA. The matrix of screened Coulomb interactions, evaluated in the framework of constrained random-phase approximation (RPA) [29], can be approximated in terms of two Kanamori parameters [30]: the intraorbital Coulomb repulsion $\mathcal{U} = 3.15$ eV and the exchange interaction $\mathcal{J} = 0.67$ eV. Then, the effective interaction responsible for the intraatomic exchange splitting between the minority- and majority-spin states can be evaluated $U = \mathcal{U} + 2\mathcal{J}$. The crystal-field splitting of atomic t_{2g} levels is about 100 meV [31]. Other parameters can be found elsewhere [32]. As we will see below, the model has serious limitations for the quantitative description of the ME effect in Cr_2O_3 . Nevertheless, we consider it for the explanatory purposes.

The corundum structure of Cr_2O_3 has four interconnected Cr sublattices, which can be antiferromagnetically arranged as A1, A2, and A3 (see Fig. 2). Among them, the magnetic space group of A1 contains the spacial inversion \hat{I} as it is, while in A2 and A3 \hat{I} is combined with the time reversal \hat{T} . Thus, the A1 structure allows for the weak ferromagnetism [2],

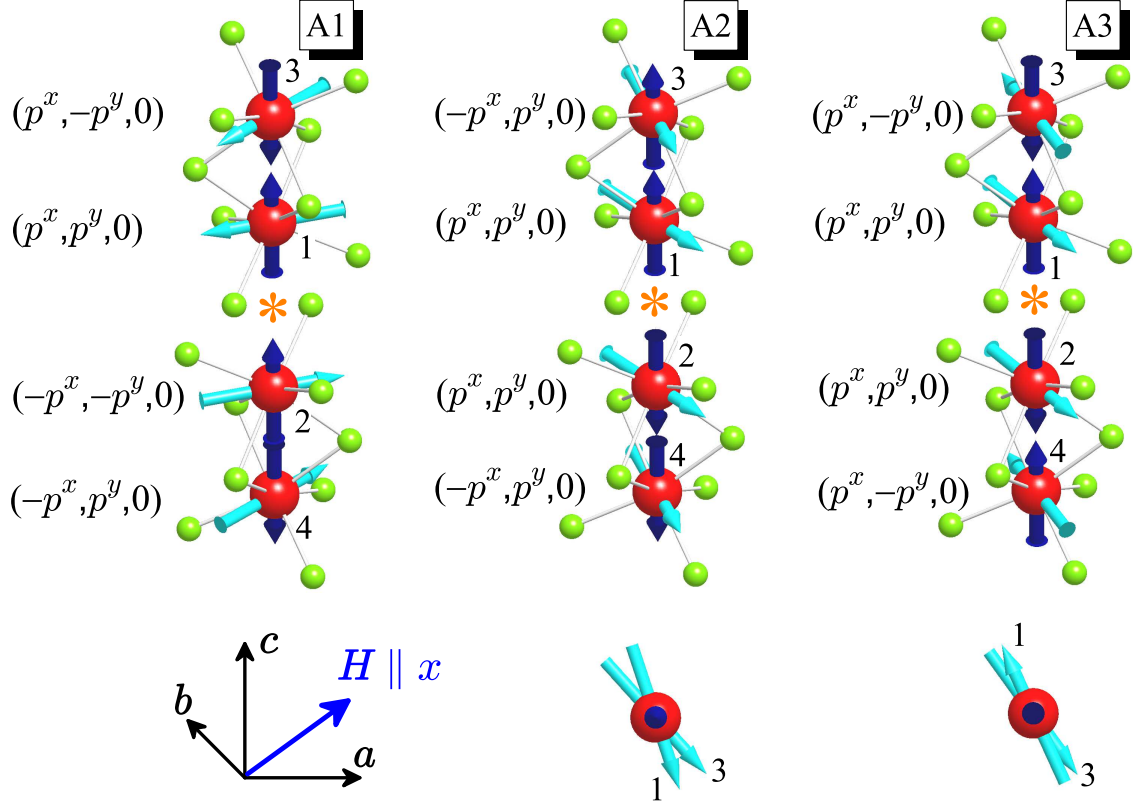


FIG. 2. (Color online) Directions of electronic polarization at four Cr sites in the primitive cell of Cr_2O_3 , which is induced by the ferromagnetic canting of spins along the x axis in three possible antiferromagnetic structures. The directions of spins are denoted by the blue (dark) arrows. The directions of electronic polarization are denoted by the cyan (light) arrows. The Cr atoms are indicated by the big red spheres and the neighboring oxygen atoms are indicated by the small green spheres. The inversion center is indicated by *. The upper panel is the side view, while the lower panel is the top view. a , b , and c denote the directions of hexagonal lattice vectors, and H denotes the external magnetic field inducing the ferromagnetic canting of spins along x . The notations $(\pm p^x, \pm p^y, 0)$ explain the symmetry properties of the induced polarization vectors $\partial \mathbf{P} / \partial e^x$ at four Cr sites. The numerical values of (p^x, p^y) are $(-0.08, 0.02)$, $(0.12, -0.57)$, and $(0.08, -0.79) \mu\text{C}/\text{m}^2$ for the antiferromagnetic structures A1, A2, and A3, respectively.

while A2 and A3 are expected to exhibit the perpendicular ME effect, when the AFM structure is deformed by the external magnetic field [4] as explained in Fig. 2. The magnetic ground state of Cr_2O_3 is A3, which was also confirmed by our calculations. The directions

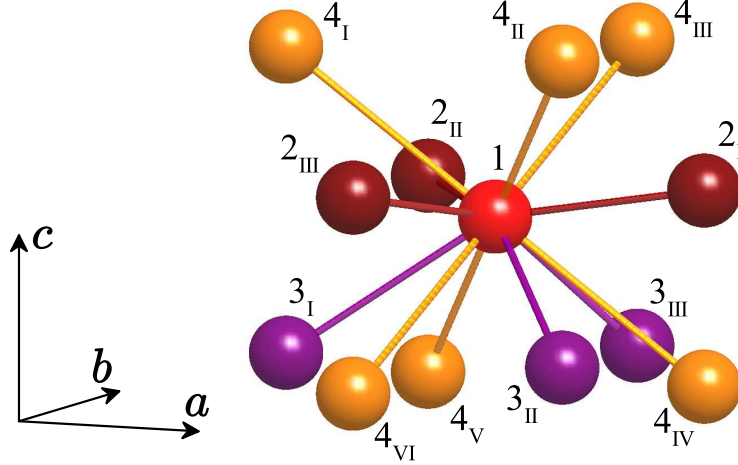


FIG. 3. (Color online) Fragment of the crystal structure of Cr_2O_3 : central Cr site of the type 1 and several coordinations spheres of the neighboring Cr sites of the types 2, 3, and 4 with the notations of their atomic positions. \mathbf{a} , \mathbf{b} , and \mathbf{c} denote the directions of hexagonal lattice vectors.

of magnetic moments are parallel to $\mathbf{c} = \mathbf{z}$.

Eqs. (8) and (10) allow us to rationalize the behavior of electronic polarization by separating the contributions of atomic pairs around each Cr site. Around site 1, the largest contributions to \mathbf{P} comes from the atomic pairs in three coordinations spheres, formed by the atoms 2, 3, and 4, which are displayed in Fig. 3, and where the notations of atomic types is the same as in Fig. 2.

First, we note that the FM bond will not contribute to the perpendicular ME effect: even in the external field \mathbf{H} such spins remain ferromagnetically aligned and, therefore, the cross product $[\mathbf{e}_i \times \mathbf{e}_j]$ will vanish. Moreover, in the case of perpendicular ME effect, the cross products $[\mathbf{e}_i \times \mathbf{e}_j]$ will be the same in all equivalent bonds.

Another important aspect is the symmetry. In order to estimate the ME coupling constant, we first evaluate the parameters \mathcal{P}_{ij} , which obey the symmetry properties of the $R\bar{3}c$ group and contains all the information about the individual symmetry of the Cr_2O_3 lattice. For instance, the pseudovectors \mathcal{P}_{ij} in the nearest-neighbor (NN) bond $\langle 13 \rangle$ (and equivalent to it bonds), parallel to the \mathbf{c} axis, will vanish due to the joint effect of the threefold rotation and the glide reflection, which transform this bond to itself. Then, for the bonds $\langle 12_I \rangle$, $\langle 13_I \rangle$, and $\langle 14_I \rangle$ (see Fig. 3) the calculated parameters \mathcal{P}_{ij} are $(-0.066, 0.007, 0)$, $(0, 0.009, 0)$, and $(-0.002, 0.010, 0)$, respectively (in $\mu\text{C}/\text{m}^2$). The parameters for other bonds can be obtained

from \mathcal{P}_{12i} , \mathcal{P}_{13i} , and \mathcal{P}_{14i} using the symmetry operations of the $R\bar{3}c$ group. Moreover, due to the threefold rotation about \mathbf{c} , we will have the following property: $\sum_j \mathcal{P}_{ij} = 0$. Nevertheless, the combination $\sum_j \epsilon_{ji} \mathcal{P}_{ij}$, which specifies the value of the electronic polarization (4), can be finite, which will lead to the finite ME effect. All these properties do not depend on the type of the AFM order and will hold for A1, A2, and A3.

Then, we consider the behavior of polarization vectors $\mathbf{p}_i = \sum_j \partial \mathcal{P}_{ij} / \partial e^x$, induced by the FM canting of spins along \mathbf{x} and associated with each magnetic site for different types of the AFM order (see Fig. 2). In the A1 phase, due to the FM alignment of spins in the bonds connecting the atomic types 1 and 2 (3 and 4), these bonds will not contribute to \mathbf{p}_i . Thus, one have to consider all possible connections of the sites 1 and 2 with the sites 3 and 4. Moreover, since the sites 1 and 2 (3 and 4) are transformed to each other by \hat{I} without flipping the directions of spins, we will have: $\hat{I} \epsilon_{ji} \mathcal{P}_{ij} = -\epsilon_{j'i'} \mathcal{P}_{i'j'}$ but $[\mathbf{e}_i \times \mathbf{e}_j] = [\mathbf{e}_{i'} \times \mathbf{e}_{j'}]$, and, therefore, $\mathbf{p}_2 = -\mathbf{p}_1$ ($\mathbf{p}_4 = -\mathbf{p}_3$), where i' (j') is the inversion image of i (j). Thus, as expected [2, 4], the FM canting of spins in the phase A1 will lead to the antiferroelectric behavior with no net polarization. Our analysis provides a transparent microscopic explanation of this effect.

In the phases A2 and A3, however, the spins 1 and 2 (3 and 4) are coupled antiferromagnetically. Therefore, these bonds will contribute to \mathbf{p}_i . Moreover, in addition to $\hat{I} \epsilon_{ji} \mathcal{P}_{ij} = -\epsilon_{j'i'} \mathcal{P}_{i'j'}$, in this case we will have: $[\mathbf{e}_i \times \mathbf{e}_j] = -[\mathbf{e}_{i'} \times \mathbf{e}_{j'}]$ (due to the $\hat{I}\hat{T}$ symmetry of the phases A2 and A3, the inversion will also flip the directions of spins) and, therefore, $\mathbf{p}_2 = \mathbf{p}_1$ ($\mathbf{p}_4 = \mathbf{p}_3$). This is a microscopic explanation of the ME effect, which is expected in the phases A2 and A3.

The direction of polarization, however, requires additional symmetry considerations, and this is the point where the external field \mathbf{H} comes into play. For instance, if (without field) all \mathbf{e}_i are parallel to \mathbf{z} and the field \mathbf{H} is parallel to \mathbf{x} (see Fig. 2), $[\mathbf{e}_i \times \mathbf{e}_j]$ will be parallel to \mathbf{y} and, according to Eq. (4), we have to consider the behavior of \mathcal{P}_{ij}^y and ϵ_{ji} under the glide reflection $\{\hat{m}_y | \mathbf{c}/2\}$ (\hat{m}_y being the mirror reflection $y \rightarrow -y$), connecting the sites 1 and 4 (2 and 3). In the A2 phase, this transformation is combined with \hat{T} and, therefore, will additionally flip the direction of spins. Then, it is straightforward to show (similar to the above considerations for \hat{I}) that $\{\hat{m}_y | \mathbf{c}/2\}$ leads to the the additional symmetry properties: $p_1^x = -p_4^x$ and $p_1^y = p_4^y$ ($p_1^x = p_4^x$ and $p_1^y = -p_4^y$) for A2 (A3). This explains why \mathbf{P} in A2 and A3 will be parallel to, respectively, \mathbf{y} and \mathbf{x} .

These behavior cannot be properly described by the phenomenological expression (2) [7, 8]: in the case of ME effect, the cross product $[\mathbf{e}_i \times \mathbf{e}_j]$ is the same for all equivalent bonds. Then, the bonds $\langle 14_I \rangle - \langle 14_{VI} \rangle$ will not contribute to \mathbf{P} because $\sum_j \boldsymbol{\epsilon}_{ji} = 0$ (see Fig. 3). For other types of bonds $\sum_j \boldsymbol{\epsilon}_{ji}$ is finite and parallel to \mathbf{z} . Therefore, according to Eq. (2), for $\mathbf{H} \parallel \mathbf{x}$ the induced polarization should be always parallel to \mathbf{x} . This could explain the direction of the polarization in the A3 phase, but not in the A2 one.

Finally, we evaluate the matrix element of the ME tensor α_{\perp} using the numerical value of $p_x = 0.08 \mu\text{C}/\text{m}^2$ for the A3 phase and the chain rule: $\alpha_{\perp} \equiv \frac{\partial P^x}{\partial H^x} = \frac{\partial P^x}{\partial e^x} \frac{\partial e^x}{\partial H^x}$, where $\frac{\partial e^x}{\partial H^x}$ is estimated using parameters of the Heisenberg model $E_H = -\sum_{i>j} J_{ij} \mathbf{e}_i \cdot \mathbf{e}_j$, obtained in the theory of infinitesimal spin rotations [19, 33], as $\frac{\partial e^x}{\partial H^x} = -\frac{M}{J_0}$ ($M \approx 3 \mu_B$ being the spin magnetic moment and $J_0 = \sum_j J_{ij} \approx -116 \text{ meV}$) [34]. It should be noted that for half-filled Mott insulators, the orbitals degrees of freedom and inactive and parameters of exchange interactions obtained in the SE theory, Eq. (6), are typically well consistent with the ones obtained in the more general theory of infinitesimal spin rotations [33]. This justifies the perturbative treatment of the transfer integrals and the crystal-field splitting in the framework of the SE theory. However, the obtained value of $\alpha_{\perp} \sim 2 \times 10^{-4} \text{ ps/m}$ is very small, which simply means that the considered spin-current effect is not the main mechanism of the ME coupling in Cr_2O_3 . This is in line with modern understanding of the ME effect in Cr_2O_3 , which is known include other important contributions beyond the considered model. Particularly, the lattice effect is very important [22, 23]. Moreover, the orbital magnetization, which is neglected in the considered half-filled t_{2g} model, can also contribute to α_{\perp} [22, 24]. We expect that much better agreement with experimental data can be obtained by considering a more general model, describing the behavior of all Cr $3d$ bands in the basis of Cr t_{2g} and e_g Wannier orbitals (see Fig. 1). For instance, we have found that the DM interactions are also strongly underestimated in the t_{2g} only model in comparison with the five-orbital model, where \mathbf{d}_{ij} can be computed using Green's function perturbation theory [27]. Apparently, the half-filled t_{2g} model is a crude approximation both for DM exchange interactions and electric polarization in Cr_2O_3 , and a more relevant microscopic model should include explicitly the effect of the e_g band. For Cr_2O_3 , it implies the consideration of several new contributions to the electronic polarization, which are no longer described by Eq. (10) at the half-filling. Below, we will consider several example of $3d^5$ compounds which are described by a more general model, which explicitly includes

both t_{2g} and e_g states at the half filling, and argue that such model generally provides much better description for the electronic polarization.

B. Linear Magnetoelectric Effect in BiFeO₃

BiFeO₃ is the well known type-I multiferroic, where the FE activity is mainly related to the off-centrosymmetric atomic displacements of Bi and O, while the magnetism originates from the half-filled 3d shell of Fe. The good aspect of BiFeO₃ is that the FE and AFM transition temperatures are high (1100 K and 650 K, respectively), which makes it promising for practical applications [5]. In the bulk, due to DM exchange interactions operating in the noncentrosymmetric $R3c$ structure, BiFeO₃ forms an incommensurate long-periodic spin spiral texture. The DM interactions overcome the effect magnetocrystalline anisotropy favoring the conventional G-type antiferromagnetism [35–37]. Nevertheless, the latter can be stabilized in the thin films of BiFeO₃, where the magnetocrystalline anisotropy can be substantially increased. An interesting aspect of the G-phase is that it allows for the linear ME effect, where the electric polarization rises linearly with the applied magnetic field, whereas in the spin-spiral phase, this effect is averaged to zero by the spin-spiral modulation. The linear ME coupling α in the BiFeO₃ films was first studied experimentally in Ref. [38]. However, the obtained value of α was rather moderate (of the order of 0.51 ps/m). The interest in this problem has reemerged again after report of giant ME coupling, being of the order of 3 V/(cm Oe) [39]. Even higher value of 24 V/(cm Oe) (corresponding to 3×10^4 ps/m [40]) was reported later in the composite films including BiFeO₃ [41].

In this section we will investigate the linear ME effect in BiFeO₃. The computational details and parameters of the model, constructed in the basis of five Fe3d states near the Fermi level, can be found in the previous publication [27].

The behavior of \mathcal{P}_{ij} can be understood on the cluster, where the central Fe site is surrounded by its six nearest neighbors (Fig. 4). In fact, other bonds also produce a sizable contribution to the ME effect in BiFeO₃. However, as expected, the main contribution comes from the nearest neighbors. Moreover, the bonds between Fe sites of the same type (either 1 or 2) are ferromagnetically coupled and, therefore, do not contribute to the ME effect (see discussions in Sec. III A). For the bond $\langle 12_I \rangle$, corresponding to $\Delta\tau_{2,1} = (-a, 0, \frac{c}{2})$ (where $a = 3.222$ Å and $c = 4.625$ Å are the rhombohedral lattice parameters), we obtain

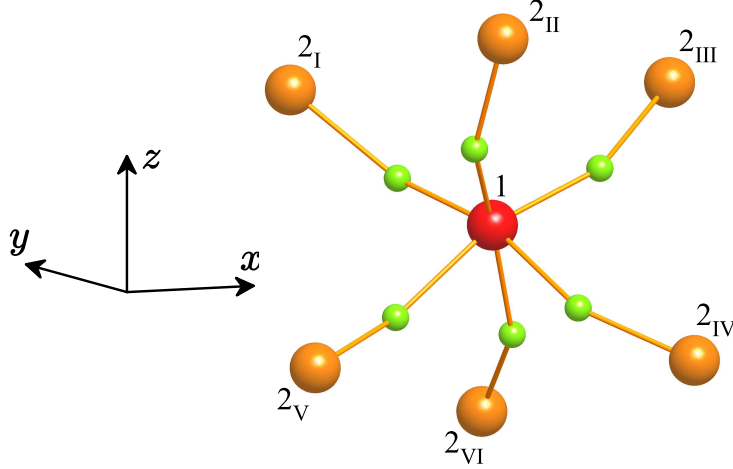


FIG. 4. (Color online) Fragment of the crystal structure of BiFeO_3 : central Fe site of the type 1 is surrounded by neighboring Fe sites of the type 2 (all are indicated by the big red spheres) with the notations of their atomic positions. \mathbf{a} , \mathbf{b} , and \mathbf{c} denote the directions of trigonal lattice vectors. The intermediate O atoms are indicated by the small green spheres.

$\mathcal{P}_{12\text{I}} = (7.88, -3.08, -1.68) \mu\text{C}/\text{m}^2$. The parameters for other bonds can be obtained using the symmetry operations of the group $R3c$, similar to the DM exchange interactions, which were considered in details in Ref. [27]. These parameters \mathcal{P}_{ij} are more than two orders of magnitude larger than the ones obtained in the t_{2g} model for Cr_2O_3 . Again, due to the threefold rotational symmetry, it holds $\sum_j \mathcal{P}_{ij} = 0$. However, when \mathcal{P}_{ij} is combined with ϵ_{ji} in Eq. (4), one can expect finite \mathbf{p}_i .

In our analysis of the ME effect, we assume that the magnetocrystalline anisotropy confines the spins in the $\mathbf{x}\mathbf{y}$ plane. To be specific, we consider here only the case of $\mathbf{L}||\mathbf{y}$, where $\mathbf{L} = \frac{M}{2}(\mathbf{e}_1 - \mathbf{e}_2)$ is the AFM order parameter (Fig. 5), but, due to the $R3c$ symmetry, similar analysis holds also for $\mathbf{L}||\mathbf{x}$. Then, we consider the effect of the magnetic field, which cants the spins in the direction of either \mathbf{z} or \mathbf{x} .

In the first case ($\mathbf{H}||\mathbf{z}$), the active component of \mathcal{P}_{ij} , which is selected by $[\mathbf{e}_1 \times \mathbf{e}_2]$, is \mathcal{P}_{ij}^x . Then, by combining it with ϵ_{ji} , using the symmetry operation of the $R3c$ group, and noting that $\frac{\partial}{\partial e_z}[\mathbf{e}_1 \times \mathbf{e}_2] = 2$, it is straightforward to show that $p_1^x \approx -16a\mathcal{P}_{12\text{I}}^y/\sqrt{4a^2 + c^2}$, while $p_1^y = p_1^z = 0$. This NN contribution accounts for 65% of total $p_1^x = -78.2 \mu\text{C}/\text{m}^2$, obtained after summation over all bonds. In the BiFeO_3 structure, the Fe sites 1 and 2 are transformed to each other by the symmetry operation $\{\hat{m}_y|(0, 0, \frac{3c}{2})\}$, which keeps the sign

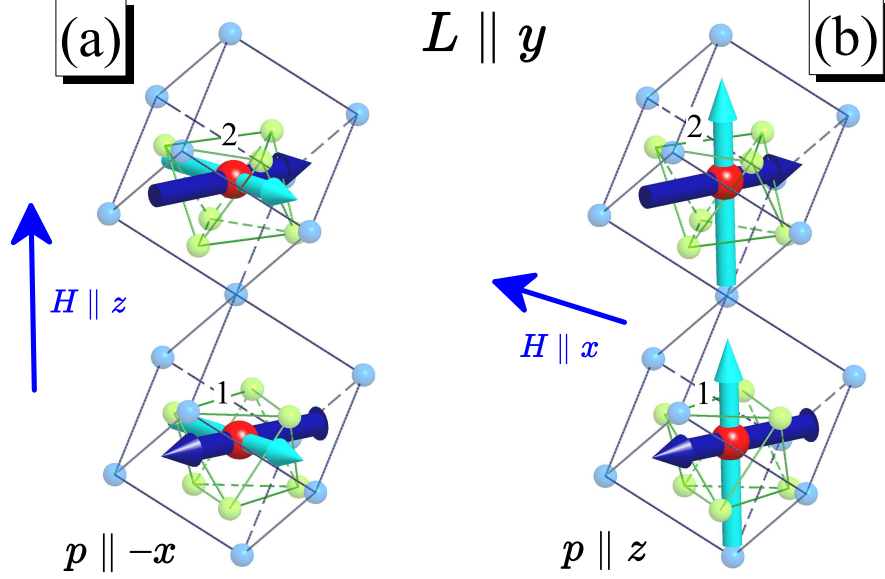


FIG. 5. (Color online) Illustration of linear magnetoelectric effect in BiFeO_3 : the spin magnetic moments (denoted by dark blue arrows) are parallel to the \mathbf{y} axis. Then, the external magnetic field along \mathbf{z} or \mathbf{x} axes induces the electric polarization (denoted by light cyan arrows) at both Fe sites of the lattices along, respectively, $-\mathbf{x}$ or \mathbf{z} . The Fe atoms are indicated by the big red spheres, the Bi atoms are indicated by the small blue spheres, and the O atoms are indicated by the small green spheres.

of ϵ^x , but changes the one of \mathcal{P}^x . Moreover, in the AFM phase, this transformation flips the directions of spins. Altogether it leads to the property $p_2^x = p_1^x$ and net electric polarization in the magnetic field.

In the second case ($\mathbf{H} \parallel \mathbf{x}$), the active component is \mathcal{P}_{ij}^z , which leads to the properties: $p_1^x = p_1^y = 0$ and $p_1^z \approx -12c\mathcal{P}_{121}^z/\sqrt{4a^2 + c^2}$ (note that in this case $\frac{\partial}{\partial \epsilon^x}[\mathbf{e}_1 \times \mathbf{e}_2] = -2$). This NN contribution accounts for 60% of total $p_1^z = 19.7 \mu\text{C}/\text{m}^2$. Similar to $\mathbf{H} \parallel \mathbf{z}$, it is straightforward to show that $p_2^z = p_1^z$, also resulting in finite ME effect.

Thus, the induced electronic polarization satisfies the condition $\mathbf{P} \sim [\mathbf{H} \times \mathbf{L}]$, being in total agreement with results of the Ginzburg-Landau theory [42]. Finally, we evaluate matrix elements of the ME tensor, $\alpha_{\parallel} = \frac{\partial P^z}{\partial H^x}$ and $\alpha_{\perp} = \frac{\partial P^x}{\partial H^z}$ (for $\mathbf{L} \parallel \mathbf{y}$), using the same procedure as for Cr_2O_3 and parameters of exchange interactions J_{ij} reported in Ref. [27], which are consistent with experimental data and reproduce the experimental value of Néel

temperature (T_N). Then, using the obtained value of $J_0 \approx -241$ meV and $M \approx 5 \mu_B$, we will find $|\alpha_{\parallel}| = 0.03$ ps/m and $|\alpha_{\perp}| = 0.12$ ps/m. These results are consistent (at least, by an order of magnitude) with direct calculations of electronic polarization for the model Hartree-Fock Hamiltonian without invoking the perturbation theory for the SO coupling, and also the experimental value of 0.51 ps/m, reported in Ref. [38]. The giant enhancement of the ME coupling, which was reported in Refs. [39, 41], probably requires additional mechanisms, such as the structural and magnetic reconstruction in the critical electric field, as was proposed in Refs. [42–44].

When the spins lie in the \mathbf{xy} plane, there is also an “intrinsic ME effect” due to the FM canting of spins ($\sim 0.5^\circ$ [27, 45]) in the direction perpendicular to \mathbf{L} , which is caused by DM exchange interactions without any magnetic field. Below T_N , it leads to the polarization change ΔP^z , which can be estimated, using the obtained values of \mathcal{P}_{ij} , as $0.2 \mu\text{C}/\text{m}^2$.

Below we will critically examine the main approximations of our theory by considering the DM exchange interactions, which can be easily computed by using other techniques. Parameters of DM interactions, obtained in the SE theory for bare $\xi_0 = 53.1$ meV, $\mathbf{d}_{12_t} = (0.106, -0.287, 0.140)$ meV agree reasonably well with $\mathbf{d}_{12_t} = (0.145, -0.418, 0.177)$ meV, derived using more general Green’s function perturbation theory method for the same model [27]. Both superexchange and Green’s function methods are the first-order theories with respect to the SO coupling. Nevertheless, the Green’s function method does not employ additional approximations, such as the perturbation theory expansion with respect to the transfer integrals and the crystal-field splitting. The reasonably good agreement obtained for the DM parameters demonstrates that such approximations are indeed justifiable. The conclusion is not so trivial because, for the five-orbital model, the $t_{2g}-e_g$ level splitting in the octahedral environment is not small, being about 1.7 eV. Nevertheless, it is smaller than the effective interaction $U \approx 5.8$ eV. Another important effect is the polarizability of the electron system by the SO interaction [27], which in our case is taken into account only approximately, by using the effective coupling $\xi = 123$ meV instead of ξ_0 , where ξ was derived by fitting results of the SCLR calculations for matrix elements of the “screened” SO interactions with different projections spins. The “screened” SO interaction includes the bare contribution as well as all the self-consistent change of the Coulomb and exchange potential, treated on the mean-field level in the first order of the SO coupling. Thus, the use of ξ instead of ξ_0 simply scales the DM parameter \mathbf{d}_{12_t} by about factor of 2. Although it cap-

tures the main tendency, it does not describe all details of $\mathbf{d}_{12\text{I}} = (0.494, -1.450, 0.330)$ meV, obtained by combining SCLR with Green's function perturbation theory, which is the most rigorous method for the evaluation of DM interactions [27]. Thus, our SE theory for the DM interactions and ME coupling is probably only semi-quantitative one. However, we believe that it should not change the main conclusions, particularly regarding the comparison with the experimental data for BiFeO₃.

Finally, we would also like to stress that the phenomenological expression (2) fails to describe the ME effect in BiFeO₃: for the canted spin structure, inherent to the ME effect, $[\mathbf{e}_i \times \mathbf{e}_j]$ is the same for all neighboring bonds surrounding each Fe site. On the other hand, it holds $\sum_j \boldsymbol{\epsilon}_{ji} = 0$. Thus, no ME effect would be expected if $\mathbf{P}_{ij} \propto \boldsymbol{\epsilon}_{ji} \times [\mathbf{e}_i \times \mathbf{e}_j]$, which is obviously not true.

C. Noncollinear spin order and ferroelectric polarization in MnWO₄

MnWO₄ has attracted a considerable attention as an example of the spin-spiral magnet, which was theoretically suggested to be multiferroic [46], where this multiferroic behavior was indeed observed experimentally [46–48], and studied in many details after that [49–52]. Finite polarization was observed in the so-called noncollinear AF2 phase which is realized in the temperature interval $7.6 \text{ K} < T < 12.5 \text{ K}$ and described by the propagation vector $\mathbf{q}_{\text{AF2}} = (-0.214, \frac{1}{2}, 0.457)$ [47]. The spins rotate in the plane formed by the monoclinic \mathbf{b} axis and one of the axes \mathbf{a}^* in the \mathbf{ac} plane (see Fig. 6), the direction of which is specified by the single-ion anisotropy. The electric polarization is parallel to \mathbf{b} axis, but can be realigned along \mathbf{a} by applying the external magnetic field parallel to \mathbf{b} . In our previous work (Ref. [18]) we have suggested that the FE activity in MnWO₄ may be related to the deformation of the spin-spiral texture, which explicitly breaks the inversion symmetry. The computational details and parameters of the effective low-energy model, constructed for the half-filled Mn3d bands of MnWO₄, can be also found in Ref. [18].

It is interesting to note that, unlike in the magnetoelectric Cr₂O₃ and BiFeO₃, the direction of polarization in MnWO₄ is described by the phenomenological model (2). Indeed, for the spin rotation plane formed by \mathbf{a}^* and \mathbf{b} , the cross product $[\mathbf{e}_i \times \mathbf{e}_j]$ is parallel to \mathbf{c}^* , which is another vector in the \mathbf{ac} plane being perpendicular to \mathbf{a}^* . Then, for $\mathbf{q}_{\text{AF2}} = (-0.214, \frac{1}{2}, 0.457)$, there are two types of neighboring bonds formed by noncollinear

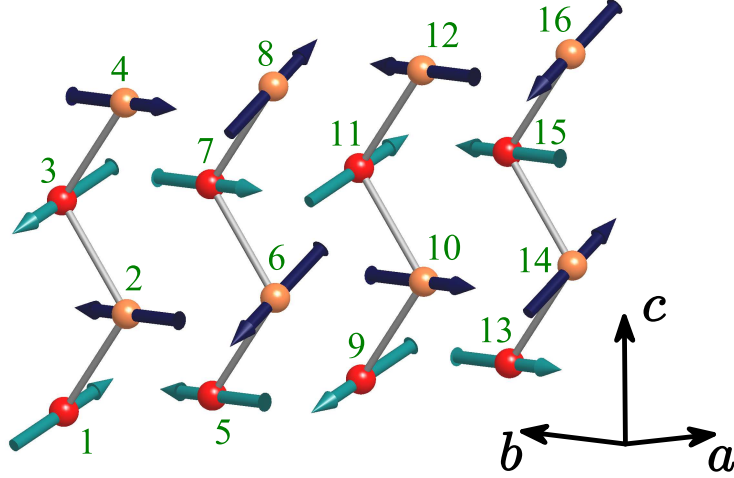


FIG. 6. (Color online) Noncollinear spin-spiral texture with $\mathbf{q} = (-\frac{1}{4}, \frac{1}{2}, \frac{1}{2})$ in MnWO_4 . \mathbf{a} , \mathbf{b} , and \mathbf{c} are the monoclinic translation vectors. Two Mn sites in the primitive cell of MnWO_4 , which are transformed to each other by the inversion operation, are indicated by red (dark) and orange (light) spheres.

spins for which $\epsilon_{ji} \parallel \mathbf{a}$ and $\epsilon_{ji} \parallel \mathbf{c}$. In both cases the expression $\mathbf{P}_{ij} \propto \epsilon_{ji} \times [\mathbf{e}_i \times \mathbf{e}_j]$ yields $\mathbf{P}_{ij} \parallel \mathbf{b}$, which agrees with the experimental situation [47]. Nevertheless, below we will show that such agreement is rather fortuitous and the actual reason behind it is the specific $P2/c$ symmetry of MnWO_4 .

The behavior of pseudovectors \mathcal{P}_{ij} , reflecting the symmetry properties of MnWO_4 , is explained in Fig. 7. The vectors are long-ranged and not restricted by the nearest neighbors. For instance, we have found sizable parameters spreading up to twelfth coordination sphere. Similar behavior was found for isotropic exchange interactions (being in total agreement with the experimental data [53]) and is related to the long-range character of the transfer integrals [18]. Due to the twofold rotation about the monoclinic \mathbf{b} axis (\hat{C}_b^2), which is one of the symmetry operations of the $P2/c$ group (apart from a translation), \mathcal{P}^y in equivalent bonds will have identical signs, while \mathcal{P}^x and \mathcal{P}^z will have opposite signs. Moreover, if the bond connect two Mn sites of the same type (either I or II), \hat{C}_b^2 will transform it to equivalent bond, separated by a translation. Therefore, for this type of bonds we will have additional condition: $\mathcal{P}^x = \mathcal{P}^z = 0$.

Then, we consider the effect of noncollinear spin-spiral texture with $\mathbf{q} = (-\frac{1}{4}, \frac{1}{2}, \frac{1}{2})$

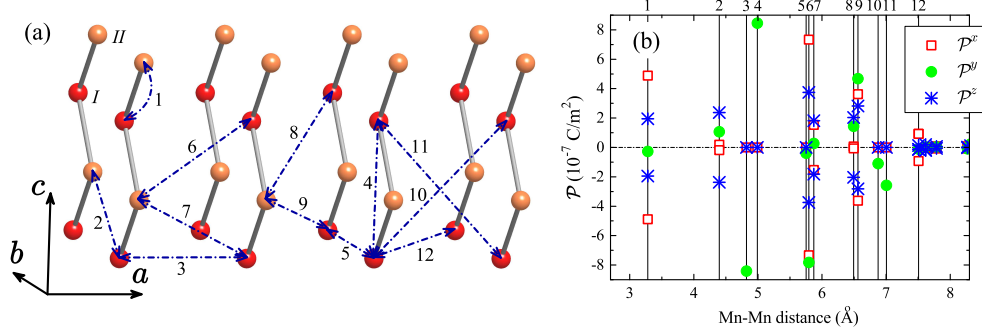


FIG. 7. (Color online) (a) Fragment of the crystal structure of MnWO_4 with explanation of the bond types surrounding Mn site *I* in twelve coordination spheres (other equivalent bonds are not shown). Two Mn sites in the primitive cell of MnWO_4 are denoted as *I* and *II*. **a**, **b**, and **c** are the monoclinic translation vectors. (b) Distance-dependence of pseudovectors $\mathcal{P} = (\mathcal{P}^x, \mathcal{P}^y, \mathcal{P}^z)$ (where $\mathbf{y} = \mathbf{b}$, $\mathbf{z} = \mathbf{c}$, and \mathbf{x} is perpendicular to \mathbf{y} and \mathbf{z}), specifying the electric polarization, in twelve coordination spheres (marked by vertical lines and numbered at the top). Due to the twofold rotation symmetry about **b**, \mathcal{P}^y in the equivalent bonds will have the same signs, while \mathcal{P}^x and \mathcal{P}^z have opposite signs, as reflected in the figure.

(Fig. 6), which is close \mathbf{q}_{AF2} realized in the experimental FE AF2 phase [47]. We will use this model mainly for numerical estimations, while our symmetry considerations are more general and valid also for the experimental \mathbf{q}_{AF2} . First we consider perfect spiral structure texture. The effect of deformation of the spin spiral, which was proposed in Ref. [18], will be investigated below.

The spin-spiral structure itself is stabilized by competing isotropic exchange interactions [18]. However, its spacial orientation depends on the single-ion anisotropy and DM interactions, which also compete with each other: the former tends to align the spins in the **ac** plane (and cant them off the **a** axis by about 40°) [18, 47], while the main DM vectors \mathbf{d}_{ij} also lie in the **ac** plane ($\in \mathbf{ac}$) [18]. Thus, in order to minimize the energy of DM interactions, some of the spins should be parallel to the **b** axis ($\parallel \mathbf{b}$), which conflicts with the small single-ion anisotropy. Moreover, the DM exchange interactions compete with the isotropic ones. Thus, the situation is indeed very subtle and the magnetic structure is rather fragile. Nevertheless, this is a very important point because, as we will see in a moment, the spacial orientation of the spin-spiral plane can control both magnitude *and* direction of

the electric polarization.

First, we consider the experimental situation where the spin-spiral plane is formed by the \mathbf{b} axis and one of directions (\mathbf{a}^*) in the \mathbf{ac} plane [47]. Then, considering the magnetic structure in Fig. 6, half of the spins is parallel to \mathbf{b} and another half belongs to \mathbf{ac} . This means that for the bonds $\langle ij \rangle$ with unparallel spins, $[\mathbf{e}_i \times \mathbf{e}_j]$ will also belong to \mathbf{ac} and, therefore, the active components of \mathcal{P}_{ij} are \mathcal{P}_{ij}^x and \mathcal{P}_{ij}^z . Then, for the equivalent bond $\langle i'j' \rangle$, which is obtained from $\langle ij \rangle$ by \hat{C}_b^2 , we will have the following properties: $\mathcal{P}_{i'j'}^x = -\mathcal{P}_{ij}^x$, $\mathcal{P}_{i'j'}^z = -\mathcal{P}_{ij}^z$, and $[\mathbf{e}_{i'} \times \mathbf{e}_{j'}] = -[\mathbf{e}_i \times \mathbf{e}_j]$. The latter property holds because \hat{C}_b^2 reverses the direction of propagation of the spin-spiral along \mathbf{a} and \mathbf{c} . Therefore, if the bond $\langle ij \rangle$ is along the propagation direction, the bond $\langle i'j' \rangle$ lies in the opposite direction. Thus, according to Eq. (4), the finite polarization is possible in the direction, which does not change under \hat{C}_b^2 , keeping the sign of corresponding projection of the vector ϵ_{ji} . For the considered geometry of the spin spiral, this direction is \mathbf{b} ($= \mathbf{y}$), in agreement with the experimental data [47]. However, the absolute value of polarization depends on the orientation of spins in the \mathbf{ac} plane. Indeed, according to Eq. (4), if $\mathbf{e}_i = (0, 1, 0)$ and $\mathbf{e}_j = (\sin \beta, 0, \cos \beta)$, the polarization behaves as $P_{ij}^y \sim (\mathcal{P}_{ij}^x \cos \beta - \mathcal{P}_{ij}^z \sin \beta)$. The dependence of total polarization $P^y = \sum_j P_{ij}^y$ on β , obtained using the numerical values of \mathcal{P}_{ij}^x and \mathcal{P}_{ij}^z , is displayed in Fig. 8. Thus, one can conclude the follows:

- (i) The finite polarization in MnWO_4 can be indeed induced by the spiral magnetic order. In this sense, the conclusion of our previous work [18] about crucial importance of inhomogeneity (or deformation) of the spin-spiral order was exaggerated;
- (ii) The absolute value of P^y strongly depends on the orientation of spins in the \mathbf{ac} plane. The maximal value of about $25 \mu\text{C}/\text{m}^2$ is comparable with experimental $50 \mu\text{C}/\text{m}^2$ [47]. However, it does not mean that this maximal value is realized for the same angle β , which minimizes the total energy of the system. In fact, the directions of spins are controlled by anisotropic interactions, which are small in MnWO_4 [18]. Therefore, the situation is very fragile. This probably explains the large spread of the values of electric polarizations reported in electronic structure calculations, which are typically underestimated in comparison with the experimental data [18, 54, 55].

Then, we consider the situation when all spins lie in the \mathbf{ac} plane and also form the spin spiral with the propagation vector $\mathbf{q} = (-\frac{1}{4}, \frac{1}{2}, \frac{1}{2})$. This behavior was observed experimentally in the magnetic field $\mathbf{H} \parallel \mathbf{b}$, which causes the spin-flop-like transition and orients the

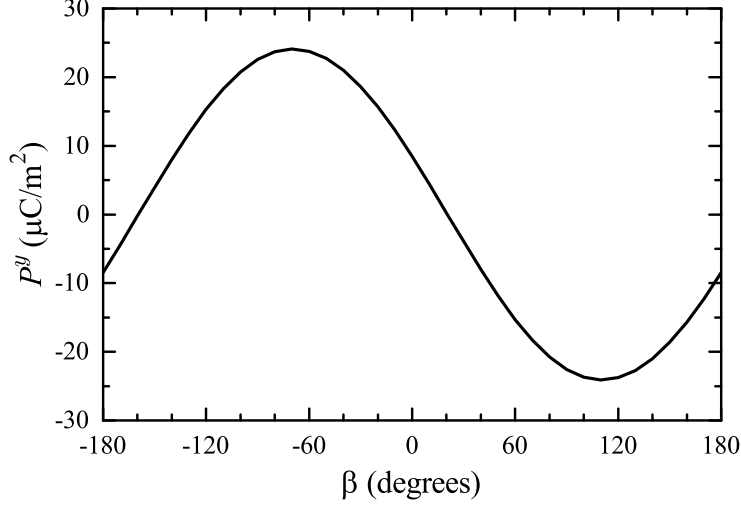


FIG. 8. Electric polarization, P^y of the spin-spiral phase of MnWO_4 with $\mathbf{q} = (-\frac{1}{4}, \frac{1}{2}, \frac{1}{2})$, where half of the spins are parallel to the monoclinic \mathbf{b} axis and another half lies in the \mathbf{ac} plane (see Fig. 6). β is the angle formed by the spins and the monoclinic \mathbf{c} axis.

spins in the \mathbf{ac} plane, also changing the direction of experimental polarization from $\mathbf{P} \parallel \mathbf{b}$ to mainly $\mathbf{P} \parallel \mathbf{a}$ [47]. In this case, $[\mathbf{e}_i \times \mathbf{e}_j]$ is parallel to \mathbf{b} and the active component of \mathcal{P}_{ij} is \mathcal{P}_{ij}^y . Then, for two bonds $\langle ij \rangle$ and $\langle i'j' \rangle$, which are transformed to each other by \hat{C}_b^2 , we will have: $\mathcal{P}_{i'j'}^y = \mathcal{P}_{ij}^y$ and $[\mathbf{e}_{i'} \times \mathbf{e}_{j'}] = -[\mathbf{e}_i \times \mathbf{e}_j]$. Therefore, the finite polarization is possible in the directions, which are reversed by \hat{C}_b^2 . This means that the polarization should lie in the \mathbf{ac} plane. The direction of polarization in the plane is not specified by the symmetry and is the matter of numerical calculations. Using the numerical values of \mathcal{P}_{ij}^y (Fig. 7), we obtain $P^x = 36.6 \mu\text{C}/\text{m}^2$ and $P^z = 9.4 \mu\text{C}/\text{m}^2$. In agreement to the symmetry arguments [51], our theory also predicts small polarization along \mathbf{c} , which could be verified experimentally. This conclusion is formally consistent with the phenomenological model (2). Nevertheless, we would like to emphasize that the actual reason for such behavior, both for $\mathbf{P} \parallel \mathbf{b}$ and $\mathbf{P} \in \mathbf{ac}$, is the specific symmetry of MnWO_4 and the existence of the twofold rotation \hat{C}_b^2 among symmetry operations of the space group $P2/c$.

Finally, we discuss the effect of spin-spiral inhomogeneity on the electronic polarization P^y in the ground state, which was proposed in Ref. [18]. This inhomogeneity is caused by the competition of isotropic and DM exchange interactions, which breaks the inversion symmetry and makes two Mn sublattices in MnWO_4 inequivalent (shown by different colors

in Ref. 6). Particularly, for the $\mathbf{q} = (-\frac{1}{4}, \frac{1}{2}, \frac{1}{2})$ structure, half of the spins will remain parallel to the \mathbf{b} axis, while another half will split in two groups, forming different angles β with respect to the \mathbf{c} axis (69° and 56° , respectively) [18]. Then, there will be four types of Mn sites with distinct neighborhood: 1, 2, 5 and 6 in Fig. 6, which yield four distinct values of $\mathbf{P}_i = \sum_j \mathbf{P}_{ij}$, respectively: 25.3, 20.0, 11.8, and 21.2 $\mu\text{C}/\text{m}^2$. The total polarization in this case is the average value of these four, yielding 19.6 $\mu\text{C}/\text{m}^2$, which is consistent with the value of electric polarization $|\mathbf{P}|$ of homogeneous spin-spiral with the average $\beta = 61.5^\circ$ (see Fig. 8). Thus, the spin-spiral inhomogeneity does not seem to make a significant effect on the value of \mathbf{P} in MnWO_4 , contrary to manganites, where the polarization is driven by nonrelativistic double exchange mechanism [14].

D. Symmetry constraints on the direction of polarization in spin-spiral MnO_2

The rutile (β -) phase of MnO_2 is another interesting example. Due to competing first- and second-neighbor AFM exchange interactions, it develops the incommensurate spin-spiral order below $T_N \approx 92$ K [56, 57]. The spin spiral propagates along the tetragonal \mathbf{c} axis ($=\mathbf{z}$). Therefore, from the viewpoint of spin-current theory, it could be another potential multiferroic compound [7, 8], though has never been considered in this context. In this section, we will show that the multiferroic effect can be indeed expected in the rutile phase of MnO_2 . Moreover, the behavior of electronic polarization obeys the phenomenological rule $\mathbf{P} \propto \mathbf{c} \times [\mathbf{e}_i \times \mathbf{e}_j]$ [7, 8]. Nevertheless, we will argue that the actual reason behind it is related to the specific $P4_2/mnm$ symmetry of MnO_2 , which imposes the symmetry constraints on the properties of \mathcal{P}_{ij} .

We use the experimental parameters of the crystal structure, reported in Ref. [58]. There are two Mn sites in the primitive cell, which are connected by the symmetry operations of the space group $P4_2/mnm$. Like in Cr_2O_3 , we consider the minimal model comprising of half-filled t_{2g} states near the Fermi level (Fig. 9). In this case, the crystal-field splitting of t_{2g} levels is pretty large (about 370 meV). The Kanamori parameters of screened intraorbital Coulomb and exchange interaction are 3.0 and 0.72 eV, respectively. Other parameters can be found elsewhere [32]. The isotropic exchange interactions between first and second neighbors, located at $(0, 0, \pm c)$ and $(\pm \frac{a}{2}, \pm \frac{a}{2}, \pm \frac{c}{2})$ (a and c being the tetragonal lattice parameters), are -16.4 meV and -12.3 meV, respectively. Like in other considered systems,

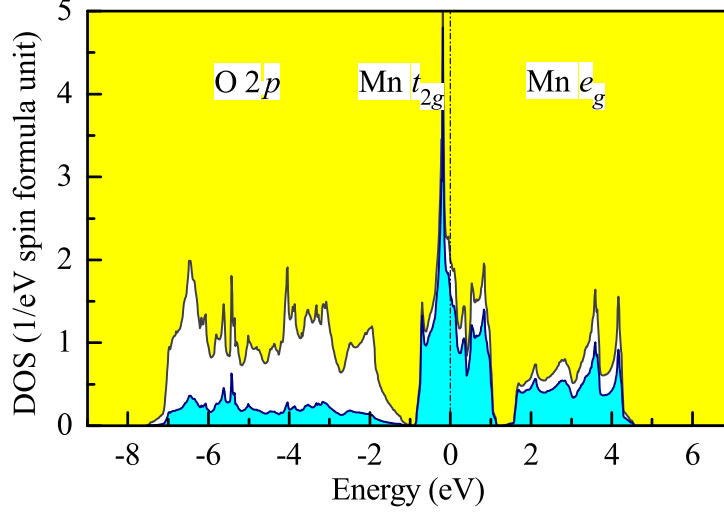


FIG. 9. (Color online) Total and partial densities of states of MnO_2 in the local density approximation. The shaded light (blue) area shows contributions of the Mn 3d states. Positions of the main bands are indicated by symbols. The Fermi level is at zero energy (shown by dot-dashed line).

the theories of SE interactions, Eq. (6), and infinitesimal spin rotations, Ref. [33], give very close values of J_{ij} . The obtained exchange interactions support the appearance of spin-spiral superstructure with $\mathbf{q} \approx (0, 0, \frac{1}{7})$ (comprising of 7 primitive cells), in agreement with the analysis of experimental data [56] and results of first-principle calculations [59]. Moreover, the magnetocrystalline anisotropy energy confines the spins in the \mathbf{xy} plane.

The $P4_2/mnm$ space group imposes the symmetry constraints on the properties of \mathcal{P}_{ij} , which are explained in Fig. 10. The parameters \mathcal{P}_{ij} between nearest neighbors vanish identically due to the mmm symmetry in the bonds $(0, 0, \pm c)$. Then, due to the symmetry operations $\{\hat{C}_c^4 | (\frac{a}{2}, \frac{a}{2}, \frac{c}{2})\}$ and $\{\hat{m}_x | (\frac{a}{2}, \frac{a}{2}, \frac{c}{2})\}$ (\hat{C}_c^4 being the fourfold rotation about the tetragonal axis \mathbf{c}), transforming the second-neighbor bonds to themselves, the corresponding parameters \mathcal{P}_{ij} will have the following form: $\mathcal{P}_{ij} = (\pm\mathcal{P}, \pm\mathcal{P}, 0)$ (see Fig. 10). Therefore, it is straightforward to see that the spin spiral, propagating along \mathbf{c} ($=\mathbf{z}$) and rotating in the \mathbf{xy} plane, does not induce any polarization because the active component \mathcal{P}_{ij}^z is identically equals to zero. For other bonds with lower symmetry, some of \mathcal{P}_{ij}^z can be finite. However, the phases of $\epsilon_{ji}\mathcal{P}_{ij}^z$ alternate for the equivalent types of bonds, again resulting in no net polarization.

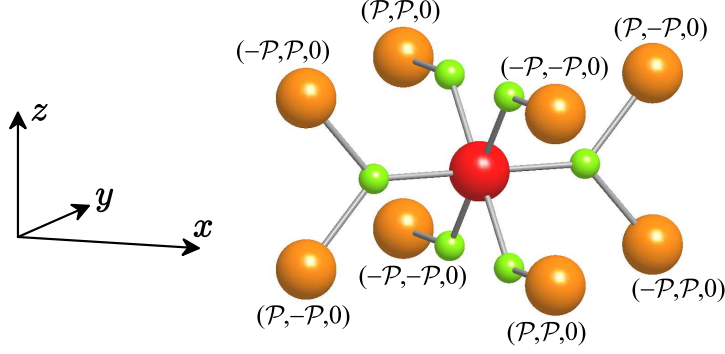


FIG. 10. (Color online) Fragment of the crystal structure of MnO_2 illustrating the symmetry properties of pseudovectors \mathbf{P}_{ij} in eight neighboring bonds, connecting two types of Mn sites. The Mn atoms are indicated by the big red spheres and the O atoms are indicated by the small green spheres. The numerical value of parameter \mathcal{P} is $0.023 \mu\text{C}/\text{m}^2$.

However, when the spins rotate in the \mathbf{yz} , the active component is \mathcal{P}_{ij}^x , which is finite. Moreover, by combining the phases of \mathcal{P}_{ij}^x with the ones of ϵ_{ji} , it is straightforward to see that $P^x = P^z = 0$, while P^y can be finite. Using obtained parameters \mathcal{P}_{ij}^x we estimate P^y for $\mathbf{q} \approx (0, 0, \frac{1}{7})$ as $2 \mu\text{C}/\text{cm}^2$. Similar conclusion holds when the spins rotate in the \mathbf{zx} plane.

Thus, we expect no FE activity in the magnetic ground state of MnO_2 . However, small polarization can be induced by rotating the spins to either \mathbf{yz} or \mathbf{zx} plane. It can be done by applying the external magnetic field along either \mathbf{x} or \mathbf{y} axis. Thus, our finding can be verified experimentally. The result is formally consistent with the phenomenological expression $\mathbf{P} \propto \mathbf{c} \times [\mathbf{e}_i \times \mathbf{e}_j]$ [7, 8]. However, it should be understood that, similar to MnWO_4 , the actual reason behind it is the specific symmetry of the rutile phase of MnO_2 .

IV. SUMMARY AND CONCLUSIONS

We have derived an analytical expression for the electronic polarization driven by the SO interaction in noncollinear magnets. For these purposes we have considered the Berry-phase theory of electric polarization and applied it to the Hubbard model at the half filling. Thus, our analysis is limited by the spin-current mechanism and do not involve additional complications caused by the orbital degrees of freedom. Moreover, all derivations are performed

in the spirit of the SE theory, which is valid in the first order of the SO coupling and in the lowest order of \hat{t}_{ij}/U , similar to the analysis of DM exchange interactions [3].

We have found that the electric polarization in each bond is given by Eq. (4), which is substantial revision of the phenomenological expression (2). Namely, the electronic polarization in Eq. (4) explicitly depends on the symmetry of the lattice (similar to the DM exchange interactions \mathbf{d}_{ij} [2]): this dependence is described by the pseudovector \mathcal{P}_{ij} , which is coupled to the cross product $[\mathbf{e}_i \times \mathbf{e}_j]$, depending on the directions of spins. Thus, this coupling describes how the symmetry of the lattice interferes with the symmetry of the noncollinear arrangement of spins. The direction of the polarization itself is specified by the unit vectors \mathbf{e}_{ji} in the direction connecting two magnetic sites, which are modulated by the scalar $\mathcal{P}_{ij} \cdot [\mathbf{e}_i \times \mathbf{e}_j]$. We argue that, even though the direction of electric polarization in some spin-spiral magnets can be described by the phenomenological expression (2), the actual reason behind it is the specific symmetry properties of each considered system, which are described by the pseudovectors \mathcal{P}_{ij} . Moreover, we have shown that the spin-current mechanism is much more generic and operates not only in spin-spiral compounds, but also in other types of noncollinear magnets, where the phenomenological expression (2) breaks down. Particularly, absolutely the same mechanism may lead to the ME effect induced by the ferromagnetic canting of spins in the external magnetic field.

Another important factor, which plays a crucial role even at the half-filling, is the crystal-field splitting. We have shown that without crystal field, both DM exchange interactions and electronic polarization will vanish. However, the crystal field may have other interesting consequences. For instance, it leads to the asphericity in the distribution of the charge density around each transition-metal site and, if the latter is located not in the centrosymmetric position (like for all considered here compounds), one can also expect ionic contribution to the electronic polarization, which can be also derived from the Berry-phase theory, as was demonstrated recently in Ref. [60] for $\text{Ba}_2\text{CoGe}_2\text{O}_7$. This is also consistent with the phenomenological analysis by Moriya [6], who expressed the total polarization as the sum of ionic contributions and the ones originating from the bonds. The ionic contributions were also evaluated in the present work and found to be at least one order of magnitude smaller than the “anomalous” pair contributions, which are given by Eq. (4) and related to fine details of the electronic structure [61].

Using parameters of the effective Hubbard model, derived from the first-principles elec-

tronic structure calculations, we have evaluated the spin-current contribution to the electronic polarization for the series of ME materials (Cr_2O_3 and BiFeO_3) and multiferroics compounds with the spin-spiral structure (MnWO_4 and MnO_2). We have shown that, although Eq. (4) excellently reproduces the symmetry properties of polarization, its numerical values can be severely underestimated, depending on the material. Particularly, the largest disagreement was found for the ME effect in Cr_2O_3 , which suggest the importance of other (lattice and orbital) contributions, in agreement with the previous finding [22–24].

We have also clarified the microscopic origin of FE activity in the spin-spiral phase of MnWO_4 : although the spin spiral in this case is deformed by competing isotropic and anti-symmetric DM exchange interactions, which explicitly breaks the inversion symmetry [18], this deformation seems to have a minor effect on the value of electronic polarization. The main contribution to the polarization comes from the spin-current term, given by Eq. (4), which also describes the change of the direction of polarization, depending on the spacial orientation of the spin spiral.

Finally, we have predicted the FE activity in the rutile phase of MnO_2 when the spin spiral is rotated out of the tetragonal xy plane.

-
- [1] A. Manchon, H. C. Koo, J. Nitta, S. M. Frolov, and R. A. Duine, *Nature Materials* **14**, 871 (2015); F. Cardano and L. Marrucci, *Nature Photonics* **9**, 776 (2015); K. Y. Bliokh, F. J. Rodríguez-Fortuño, F. Nori, and A. V. Zayats, *ibid.* **9**, 796 (2015); E. I. Rashba, *J. Phys.: Condens. Matter* **28**, 421004 (2016).
 - [2] I. Dzyaloshinsky, *J. Chem. Phys. Solids* **4**, 241 (1958).
 - [3] T. Moriya, *Phys. Rev.* **120**, 91 (1960).
 - [4] I. E. Dzyaloshinskii, *J. Exp. Theor. Phys.* **37**, 881 (1959).
 - [5] T. Kimura, *Annu. Rev. Mater. Res.* **37**, 387 (2007); S.-W. Cheong and M. Mostovoy, *Nature Materials* **6**, 13 (2007); D. Khomskii, *Physics* **2**, 20 (2009); Y. Tokura and S. Seki, *Adv. Mater.* **22**, 1554 (2010).
 - [6] T. Moriya, *J. Appl. Phys.* **39** 1042 (1968).
 - [7] H. Katsura, N. Nagaosa, and A. V. Balatsky, *Phys. Rev. Lett.* **95**, 057205 (2005).
 - [8] M. Mostovoy, *Phys. Rev. Lett.* **96**, 067601 (2006).

- [9] I. A. Sergienko and E. Dagotto, Phys. Rev. B **73**, 094434 (2006).
- [10] R. D. King-Smith and D. Vanderbilt, Phys. Rev. B **47**, 1651 (1993); D. Vanderbilt and R. D. King-Smith, *ibid.* **48**, 4442 (1993).
- [11] R. Resta, J. Phys.: Condens. Matter **22**, 123201 (2010).
- [12] N. Marzari, A. A. Mostofi, J. R. Yates, I. Souza, and D. Vanderbilt, Rev. Mod. Phys. **84**, 1419 (2012).
- [13] P. Barone, K. Yamauchi, and S. Picozzi, Phys. Rev. Lett. **106**, 077201 (2011).
- [14] I. V. Solovyev and S. A. Nikolaev, Phys. Rev. B **87**, 144424 (2013); I. V. Solovyev and S. A. Nikolaev, Phys. Rev. B **90**, 184425 (2014).
- [15] K. Yamauchi and P. Barone, J. Phys.: Condens. Matter **26**, 103201 (2014).
- [16] I. V. Solovyev, Phys. Rev. B **83**, 054404 (2011); **90**, 179910(E) (2014).
- [17] W. C. Koehler, J. W. Cable, M. K. Wilkinson, and E. O. Wollan, Phys. Rev. **151**, 414 (1966); G. P. Felcher, G. H. Lander, T. Arai, S. K. Sinha, and F. H. Spedding, Phys. Rev. B **13**, 3034 (1976).
- [18] I. V. Solovyev, Phys. Rev. B **87**, 144403 (2013).
- [19] I. V. Solovyev, J. Phys.: Condens. Matter **20**, 293201 (2008).
- [20] P. W. Anderson, Phys. Rev. **115**, 2 (1959).
- [21] A. Malashevich and D. Vanderbilt, Phys. Rev. Lett. **101**, 037210 (2008); Phys. Rev. B **80**, 224407 (2009).
- [22] A. Malashevich, S. Coh, I. Souza, and D. Vanderbilt, Phys. Rev. B **86**, 094430 (2012).
- [23] E. Bousquet, N. A. Spaldin, and K. T. Delaney, Phys. Rev. Lett. **106**, 107202 (2011).
- [24] A. Scaramucci, E. Bousquet, M. Fechner, M. Mostovoy, and N. A. Spaldin, Phys. Rev. Lett. **109**, 197203 (2012).
- [25] Supplemental materials [details of derivations of parameters of DM interactions and electronic polarization in the framework of the SE theory].
- [26] O. K. Andersen, Phys. Rev. B **12**, 3060 (1975).
- [27] I. V. Solovyev, Phys. Rev. B **90**, 024417 (2014).
- [28] We use the experimental lattice parameters, reported by P. J. Brown, J. B. Forsyth, E. Lelièvre-Berna, and F. Tasset, J. Phys: Cond. Mat. **14**, 1957 (2002).
- [29] F. Aryasetiawan, M. Imada, A. Georges, G. Kotliar, S. Biermann, and A. I. Lichtenstein, Phys. Rev. B **70**, 195104 (2004).

- [30] J. Kanamori, Prog. Theor. Phys. **30**, 275 (1963).
- [31] I. V. Solovyev, Phys. Rev. B **73**, 155117 (2006).
- [32] All model parameters are available upon request.
- [33] A. I. Liechtenstein, M. I. Katsnelson, V. P. Antropov, and V. A. Gubanov, J. Magn. Magn. Mater. **67**, 65 (1987).
- [34] The corresponding Néel temperature, estimated in the framework of Tyablikov’s RPA [S. V. Tyablikov, *Methods of Quantum Theory of Magnetism* (Nauka, Moscow, 1975)] using the obtained parameters J_{ij} for Cr_2O_3 , is $T_N = 250$ K, which is in fair agreement with the experimental value of 308 K [E. J. Samuelsen, M. T. Hutchings, and G. Shirane, Physica B **48**, 13 (1970)].
- [35] I. Sosnowska and A. K. Zvezdin, J. Magn. Magn. Matter. **140-144**, 167 (1995).
- [36] J. Jeong, E. A. Goremychkin, T. Guidi, K. Nakajima, G. S. Jeon, S.-A. Kim, S. Furukawa, Y. B. Kim, S. Lee, V. Kiryukhin, S. W. Cheong, and J.-G. Park, Phys. Rev. Lett. **108**, 077202 (2012).
- [37] M. Matsuda, R. S. Fishman, T. Hong, C. H. Lee, T. Ushiyama, Y. Yanagisawa, Y. Tomioka, and T. Ito, Phys. Rev. Lett. **109**, 067205 (2012).
- [38] J.-P. Rivera and H. Schmid, Ferroelectrics **204**, 23 (1997).
- [39] J. Wang, J. B. Neaton, H. Zheng, V. Nagarajan, S. B. Ogale, B. Liu, D. Viehland, V. Vaithyanathan, D. G. Schlom, U. V. Waghmare, N. A. Spaldin, K. M. Rabe, M. Wuttig, and R. Ramesh, Science **299**, 1719 (2003).
- [40] T. Stevenson, J. Bennett, A. P. Brown, T. Wines, A. J. Bell, R. I. Smith, and T. P. Comyn, APL Materials **2**, 086105 (2014).
- [41] M. Lorenz, G. Wagner, V. Lazenka, P. Schwinkendorf, H. Modarresi, M. J. Van Bael, A. Vantomme, K. Temst, O. Oeckler, and M. Grundmann, Appl. Phys. Lett. **106**, 012905 (2015).
- [42] A. F. Popkov, M. D. Davydova, K. A. Zvezdin, S. V. Solov’yov, and A. K. Zvezdin, Phys. Rev. B **93**, 094435 (2016).
- [43] S. Lisenkov, I. A. Kornev, and L. Bellaiche, Phys. Rev. B **79**, 012101 (2009).
- [44] N. Kulagin, A. Popkov, S. Solovev, K. Sukmanova, and A. Zvezdin, Phys. Solid State **57**, 933 (2015).
- [45] C. Ederer and N. A. Spaldin, Phys. Rev. B **71**, 060401 (2005).
- [46] O. Heyer, N. Hollmann, I. Klassen, S. Jodlauk, L. Bohatý, P. Becker, J. A. Mydosh, T. Lorenz,

- and D. Khomskii, J. Phys.: Condens. Matter **18**, L471 (2006).
- [47] K. Taniguchi, N. Abe, T. Takenobu, Y. Iwasa, and T. Arima, Phys. Rev. Lett. **97**, 097203 (2006).
 - [48] A. H. Arkenbout, T. T. M. Palstra, T. Siegrist, and T. Kimura, Phys. Rev. B **74**, 184431 (2006).
 - [49] H. Mitamura, T. Sakakibara, H. Nakamura, T. Kimura, and K. Kindo, J. Phys. Soc. Jpn. **81**, 054705 (2012).
 - [50] I. Urcelay-Olabarria, E. Ressouche, A. A. Mukhin, V. Yu. Ivanov, A. M. Kadomtseva, Yu. F. Popov, G. P. Vorobev, A. M. Balbashov, J. L. García-Muñoz, and V. Skumryev, Phys. Rev. B **90**, 024408 (2014).
 - [51] I. Urcelay-Olabarria, J. L. García-Muñoz, and A. A. Mukhin, Phys. Rev. B **91**, 104429 (2015).
 - [52] Y. Xiao, C. M. N. Kumar, S. Nandi, Y. Su, W. T. Jin, Z. Fu, E. Faulhaber, A. Schneidewind, and Th. Brückel, Phys. Rev. B **93**, 214428 (2016).
 - [53] F. Ye, R. S. Fishman, J. A. Fernandez-Baca, A. A. Podlesnyak, G. Ehlers, H. A. Mook, Y. Wang, B. Lorenz, and C. W. Chu, Phys. Rev. B **83**, 140401(R) (2011).
 - [54] C. Tian, C. Lee, H. Xiang, Y. Zhang, C. Payen, S. Jobic, and M.-H. Whangbo, Phys. Rev. B **80**, 104426 (2009).
 - [55] K. V. Shanavas, D. Choudhury, I. Dasgupta, S. M. Sharma, and D. D. Sarma, Phys. Rev. B **81**, 212406 (2010).
 - [56] A. Yoshimori, J. Phys. Soc. Jpn. **14**, 807 (1959).
 - [57] H. Sato, T. Enoki, M. Isobe, and Y. Ueda, Phys. Rev. B **61**, 3563 (2000).
 - [58] A. A. Bolzan, C. Fong, B. J. Kennedy, and C. J. Howard, Australian Journal of Chemistry, **46**, 939 (1993).
 - [59] J. S. Lim, D. Saldana-Greco, and A. M. Rappe, Phys. Rev. B **94**, 165151 (2016).
 - [60] I. V. Solovyev, Phys. Rev. B **91**, 224423 (2015).
 - [61] S. Picozzi, K. Yamauchi, B. Sanyal, I. A. Sergienko, and E. Dagotto, Phys. Rev. Lett. **99**, 227201 (2007).